Cathodic pre-polarization studies on the carbon felt/KOH interface: An efficient metal-free electrocatalyst for hydrogen generation

M. Ifires, A. Addad, Alexandre Barras, T. Hadjersi, R. Chegroune, Sabine Szunerits, Rabah Boukherroub, M.A. Amin

Version of Record: https://www.sciencedirect.com/science/article/pii/S0013468621002711
Manuscript_7345b33d6cabdc537f68dacb6b911d42

Cathodic pre-polarization studies on the carbon felt/KOH interface: An efficient metal-free electrocatalyst for hydrogen generation

Madjid Ifires,[1,2,3] Ahmed Addad,[4] Alexandre Barras,[1] Toufik Hadjersi,[2] Redouane Chegroune,[3] Sabine Szunerits,[1] Rabah Boukherroub[1]*, Mohammed A. Amin[5]*

[1]*Univ. Lille, CNRS, Centrale Lille, Univ. Polytechnique Hauts-de-France, UMR 8520 – IEMN, F-59000 Lille, France*

[2]*Research Center of Semiconductor Technology for Energy-2, Bd Frantz Fanon, BP 140, Alger 7 Merveilles 16038, Algiers, Algeria*

[3]*Mechanical and Process Engineering Faculty, Department of Material Science, USTHB, B.P. 32 El-Alia, 16111, Bab- Ezzouar, Algeria*

[4]*Univ. Lille, CNRS, UMR 8207 – UMET, F-59000 Lille, France*

[5]*Department of Chemistry, College of Science, Taif University, P.O. Box 11099, Taif 21944, Saudi Arabia*

*To whom correspondence should be addressed: mohamed@tu.edu.sa (Mohammed A. Amin); rabah.boukherroub@univ-lille.fr (R. Boukherroub)

Abstract

The recent decades have witnessed a booming research effort on the development of highly active electrode materials in electrocatalysis with the aim to replace the commonly used noble metal-based ones. Although non-noble metal electrodes can fulfill some requirements in terms of performance and price, their stability in alkaline media is generally weak. Additionally, from the environmental view point, the use of metals can cause water contamination. Therefore, the preparation of metal-free electrocatalysts represents an appealing approach to overcome of the above-mentioned shortcuts. In this work, we used a simple electrochemical activation process, chronoamperometry measurements conducted in 1 M KOH at various overpotentials (-2, -2.5, -3, and -4 V *vs.* RHE) and pre-polarization periods (0.5, 2, 4, and 12h), of commercially available and cheap carbon felt (CF) electrode to achieve good performance for hydrogen evolution reaction (HER) in alkaline media. Under optimized operating conditions (12h of chronoamperometry measurement acquired at an overpotential of -4 V *vs.* RHE), the CF electrode exhibited an overpotential of 182 mV at 10 mA/cm^2, a value surpassing that recorded for the most efficacious metal-free HER electrocatalysts published in the literature. The two CF samples exposed to 12 h of cathodic activation at -2.5 and -3.0 V *vs.* RHE recorded respectively Tafel slope (b_c) values of 110 and 126 mV dec^{-1}. These b_c values are close to the standard b_c value of 120 mV dec^{-1}, suggesting the Volmer step as the main step controlling the HER. Increasing the applied cathodic potential to -4.0 V *vs.* RHE further decreased the b_c value to 90 mV dec^{-1}, referring to increased accessible active catalytic sites for the HER. The cathodically activated CF surface's morphology and composition were assessed by scanning electron microscopy (SEM) and X-ray photoelectron spectroscopy (XPS) examinations. Raman spectroscopy was also conducted to assess the influence of the cathodic activation process on the structural defects/disorder of the CF surface. The formation of oxygen-containing groups on the CF surface after cathodic activation, as evidenced from XPS analysis, is believed to enhance water adsorption and act as active sites for hydrogen generation. The technique developed herein is simple and straightforward and can be easily implemented for almost any type of electrode.

Keywords: Electrocatalysis; Hydrogen evolution reaction; Carbon felt; Cathodic activation; Alkaline electrolytes

1. Introduction

In recent years, there has been a continuous shift towards the development of clean and renewable energy sources to limit the dependence on fossil fuels, but also to minimize the impact on the environment [1]. In this context, tremendous efforts have been put on the search for highly efficient fuel cells, new metal-air batteries, and more effective production approaches of energy carriers such as hydrogen (H_2) [1, 2]. All these technologies require development of high-performance, cost-effective, and earth abundant heterogeneous electrocatalysts [2]. H_2, as a promising and valuable energy source, has received increasing attention in the last decade with a plenty of studies focused on the catalyst preparation, hydrogen precursors and cell design [2]. Water electrolysis, i.e., hydrogen evolution reaction (HER), was recognized as an interesting strategy to fulfill the needs in the development of renewable and energy conversion devices. HER is a two-electron electrocatalytic process that produces H_2 as a final product from H^+ in acidic media or H_2O from basic media, as underlined in **Table 1** [3]:

Table 1. Water electrolysis in acid and alkaline media.

Electrolyte	Water electrolysis
Acidic solution	Cathode: $2H^+ + 2e^- \rightarrow H_2$ Anode: $H_2O \rightarrow 2H^+ + ½O_2 + 2e^-$
Alkaline solution	Cathode: $2H_2O + 2e^- \rightarrow H_2 + 2OH^-$ Anode: $2OH^- \rightarrow H_2O + ½O_2 + 2e^-$

The rate determining step in HER can be inferred from the Tafel analysis [4].

Platinum (Pt) and its composites are the most performing catalysts for HER in acidic media, owing to their low onset potential, high exchange current densities and a Tafel slope of about 30 dec^{-1} [4]. In contrast, the reaction in alkaline media is hindered by the strong Pt-H

binding energy, and Pt poisoning susceptibility by underpotential deposition in the presence of trace metal ions in the electrolyte solution. Therefore, the reaction rate is decreased by more than one order of magnitude, recording higher Tafel slope values (50-150 dec^{-1}). Additionally, the high price of Pt and its low abundance favored a search for alternative catalysts with a performance comparable to that of Pt in acidic media and surpassing it in alkaline condition.

Therefore, the last decade has witnessed a huge load of research investigations on the development of metal-free electrocatalysts for overall water splitting [5, 6]. In this context, carbon-based materials, commonly used as catalyst supports, represent an outstanding class of electrodes for HER in acidic and alkaline media, owing to their high stability, high abundance, good electronic conductivity, and low cost. These multiple benefits have boosted their utilization in many electrochemical processes for sustainable energy applications [5, 6]. Among these carbon materials, carbon nanotubes, graphene and biomass-derived carbon are the most investigated electrode materials [5, 6]. Despite the interest of the carbon-based electrodes in electrolysis, the as-prepared materials are commonly less efficient for HER. Thus, many strategies have been designed to improve their electrocatalytic performance. These include heteroatom doping (mono- and multi-atom), surface functionalization, structural defect engineering, etc. [5-11].

Another elegant approach to improve the catalytic performance of carbon-based electrodes for advancing the field of metal-free HER is the cathodic activation. This method not only offers the advantage of being environmentally-friendly, it also takes place in the same electrochemical cell used for HER measurements, limiting additional costs. Despite these benefits, cathodic activation of carbon-based materials is scarce in the literature. Early study by Prosini *et al.* revealed that cathodic polarization of CNTs substrate allowed to improve its electrocatalytic activity for HER [12]. Das *et al.* demonstrated that cycling single-wall carbon

nanotubes (SWNT) film in H_2SO_4 at 50 mV/s (+0.2 to -0.7 V *vs.* NHE), followed by a long soak time allowed to achieve a high performance for HER. The activation process was believed to be due to H_2SO_4 intercalation within the nanotubes [13]. Cui and coworkers found that a two-step activation process of multi-walled carbon nanotubes (MWCNTs), consisting of 4 h oxidation in HNO_3 at 120°C, followed by cathodic activation at -2 V *vs.* saturated calomel electrode (SCE) for 4 h in H_2SO_4, enhanced considerably the electrocatalytic properties for HER of the substrate [14]. Cathodic activation of mesoporous bacterium-derived carbon electrocatalysts (-2 V *vs.* SCE for 4 h) in 0.1 M H_2SO_4 improved their HER performance, delivering a Tafel slope of 58.4 mV dec^{-1}, an onset overpotential of 76 mV, and an exchange current density of 1.72 10^{-2} mA cm^{-2} [15]. The enhanced HER activity was ascribed to surface oxidation during the cathodic process, introducing oxygen containing groups which could act as proton acceptors/relays to facilitate H_2 evolution. Some of us have found that a cathodic cycling at -2 V in 0.5 M H_2SO_4 of Au-Pd NPs/rGO electrode led to enhanced HER activity. Even though this phenomenon was highly reproducible, its origin was not very clear [16].

Unlike carbon nanotubes and graphene, carbon felt (CF) has been mostly investigated as a carbon support for different metal and metal oxide nanoparticles for HER [17-21], owing to its open and free-standing structure, high stability in corrosive media and low cost [22, 23]. Even though CF exhibits unique benefits as a support, its catalytic activity is not recognized to be sufficient to drive effectively various electrochemical processes [22, 23]. Therefore, its activation might represent an appealing mean to explore all the benefits of this material and realize metal-free electrocatalysis.

In this study, we report for the first time the electrochemical activation of CF in 1.0 M KOH aqueous solution with the aim to improve its catalytic performance. A systematic investigation of the influence of various operating pre-polarization parameters such as applied

cathodic potential and polarization time was carried out to find the better conditions. Under optimized conditions, the CF cathodically polarized at -4.0 V *vs.* RHE for 12 h achieved a high exchange current density of 0.1 mA cm^{-2} and a Tafel slope value as low as 90 mV dec^{-1}. Additionally, it required an overpotential of 180 mV *vs.* RHE to deliver 10 mA cm^{-2}. Interestingly, the CF experienced enhanced activation during a continuous cycling stability test. Based on XPS analysis, it is hypothesized that cathodic activation induces surface oxidation. The generation of oxygen functional groups could serve as catalytic sites for protons adsorption and their effective reduction to H_2.

2. Experimental section

Electrochemical measurements

Electrochemical measurements were performed in a standard 200 mL three-electrode cell comprising Hg/HgO, NaOH (0.1 M) (Princeton Applied Research) and a graphite rod (Sigma-Aldrich, 99.999%) reference and auxiliary electrodes using an Autolab (PGSTAT30/FRA system, Ecochemie, The Netherlands) potentiostat. The reference electrode was immersed in a Luggin capillary (Princeton Applied Research) filled with 2 M potassium nitrate (KNO_3, Sigma Aldrich) solution. This capillary acts as the salt bridge to minimize the junction potentials, and inhibit contamination of the test solution with traces of mercury from the reference electrode. The working electrode (WE), namely the CF sample, was first activated through chronoamperometry, CA, (current *vs.* time at a fixed cathodic potential) measurements conducted under various conditions of cathodic pre-treatment processes, namely applied cathodic voltage and pre-polarization time.

Linear sweep voltammetry (LSV) and electrochemical impedance spectroscopy (EIS) techniques were then employed to assess the HER catalytic activity of the cathodically-activated CF samples. The long-term stability and durability tests were carried out using continuously repeated potential cycling (up to 10000 cycles) employing cyclic voltammetry

(CV) technique and CA measurements performed at a cathodic overpotential of -2.0 V *vs.* RHE for 24 h. CA technique was also applied to estimate the cathodically-activated CF catalysts' HER Faradaic efficiency (FE%) values.

The cathodically-activated CF electrocatalysts' Faradaic efficiency (*FE%*) values toward the HER were determined by measuring the volume of H_2, $(V_{H2})_{measured}$, evolved through a controlled galvanostatic electrolysis, conducted in KOH (1.0 M) for 1.0 h at room temperature, by a gas chromatograph (GC). The (*FE%*) value was then calculated from the ratio $(V_{H2})_{measured}$ / $(V_{H2})_{calculated}$, where $(V_{H2})_{calculated}$ denotes the anticipated volume of H_2 theoretically calculated during that electrolysis. The employed electrochemical techniques and *FE%* calculation are fully described in ***Section S1*** (**Supporting Information**).

3. Results and discussion

3.1. Electrochemical measurements

3.2.1. Effect of cathodic pre-treatment on the HER catalytic activity

Figure 1 shows the cathodic polarization curves recorded for as-received CF in 1.0 M KOH solution under the effect of various potential sweep rates using a new fresh electrode for each experiment. It is obvious from **Figure 1** that the polarization response is sensitive to the potential sweep rate, the cathodic current density enhances by slowing it down.

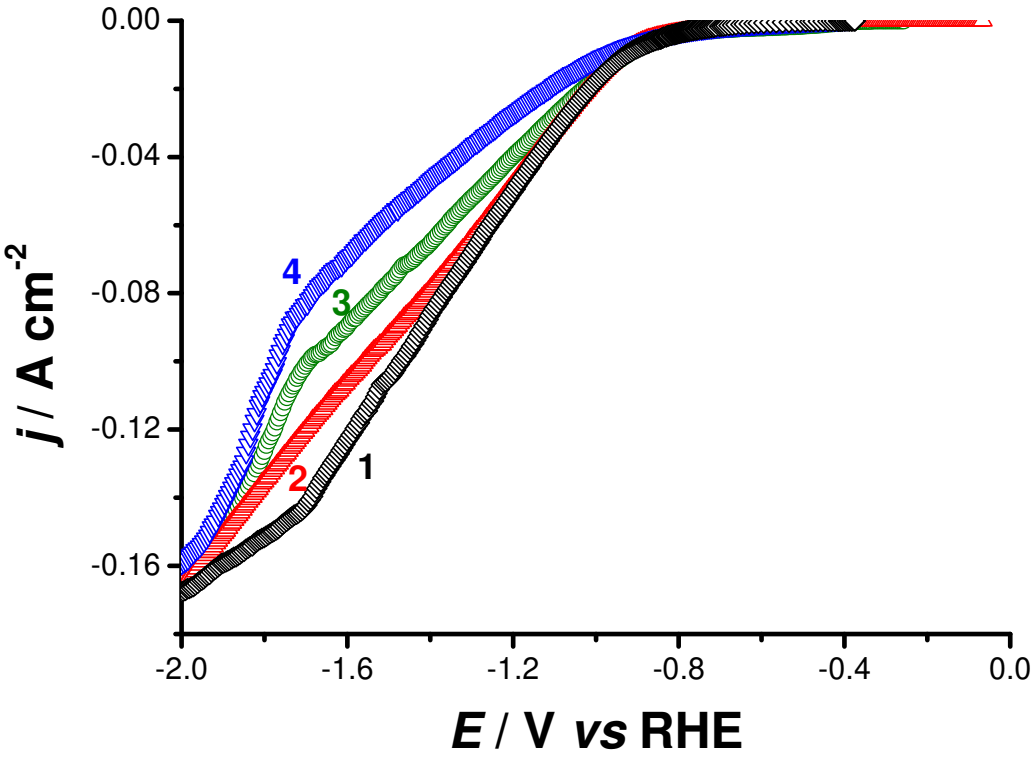

Figure 1. Cathodic polarization plots acquired for the as-received CF sample in deaerated 1.0 M KOH aqueous solution using different potential sweep rates (5-100 mV s^{-1}) at room temperature: (1) 5.0 mV s^{-1}; (2) 25 mV s^{-1}; (3) 50 mV s^{-1}; (4) 100 mV s^{-1}.

These findings encouraged us to study the influence of the polarization time (t_{pp}: 0.5 – 12 h), by holding the WE's potential at a fixed negative value, -2.0 V *vs.* RHE, **Figure 2(a)**, prior to recording the LSV curve. The effect of the applied cathodic potential at a fixed duration period on the cathodic polarization responses of the CF electrode was also studied, **Figure 3(b)**.

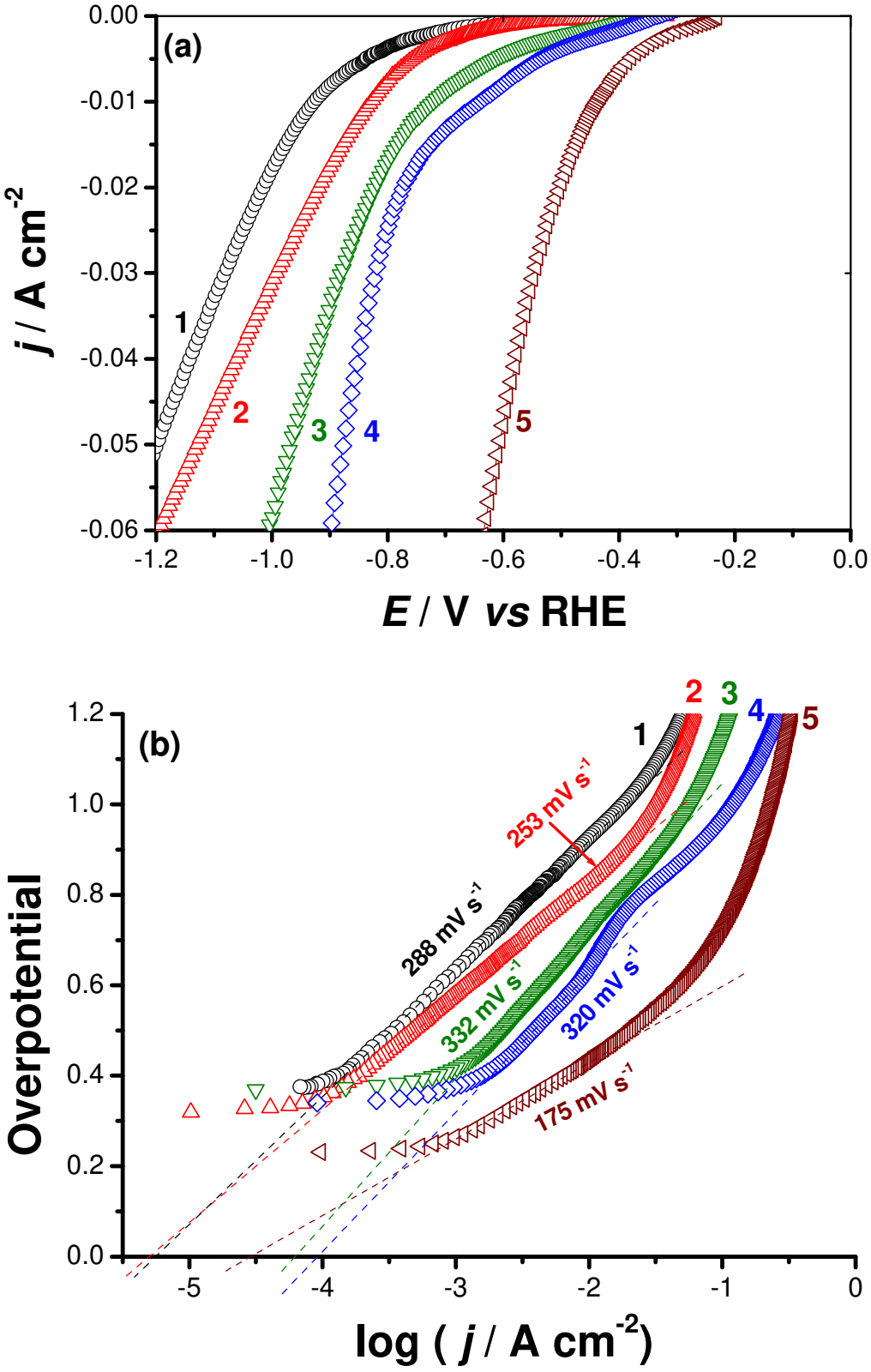

Figure 2. (**a**) Linear cathodic polarization curves acquired for the as-received CF sample after holding it at a cathodic potential of -2.0 V *vs.* RHE for various duration periods (0.5-12 h). (**b**) Fitting the experimental polarization data with Tafel equation. Measurements were performed in deaerated 1.0 M KOH solution at 5.0 mV s^{-1} at room temperature. (1) 0.0 h; (2) 0.5 h; (3) 2 h; (4) 4 h; (5) 12 h.

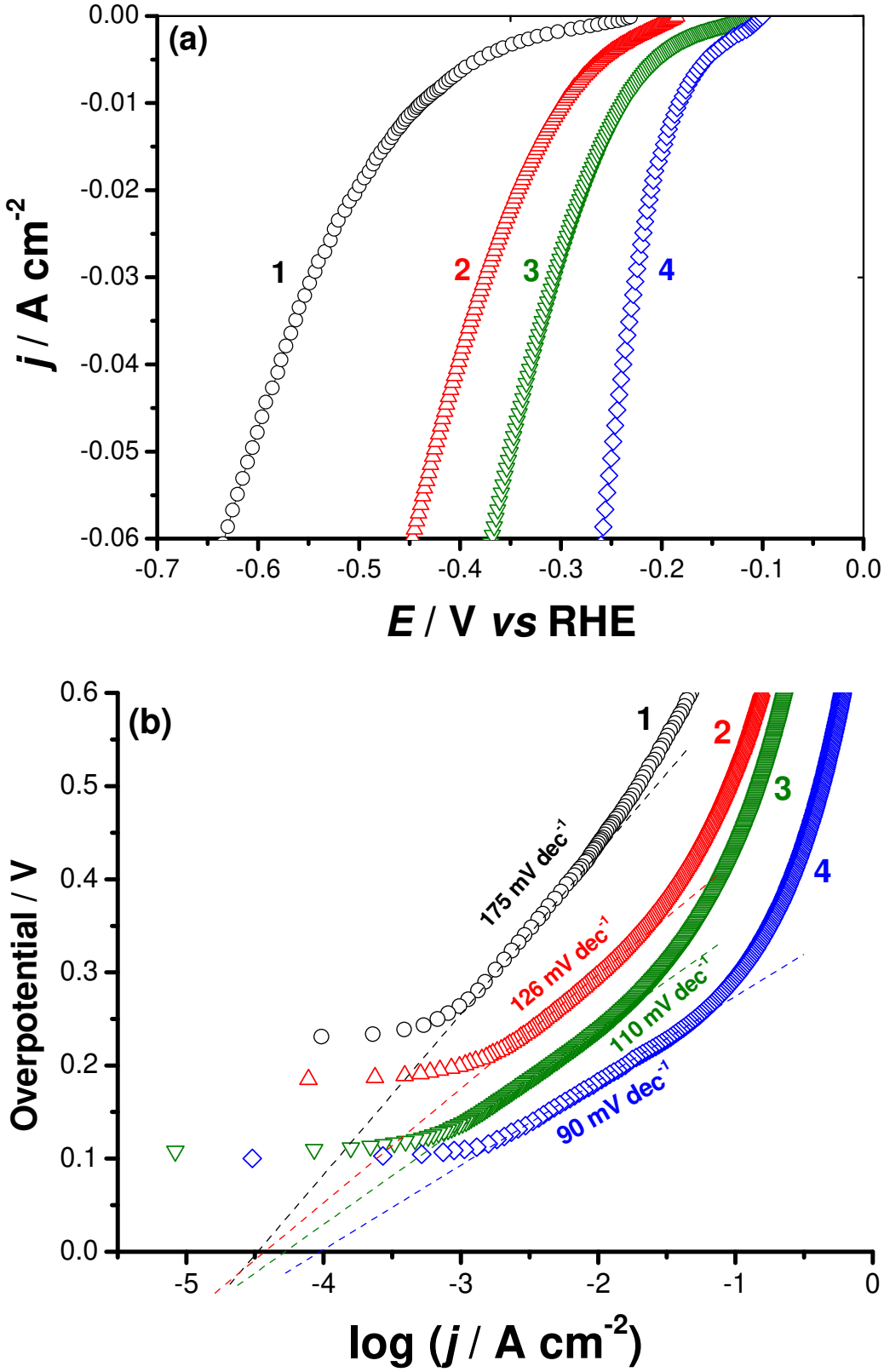

Figure 3. (**a**) Linear cathodic polarization curves acquired for the as-received CF sample after holding it at various cathodic potentials for 12 h. (**b**) Fitting the experimental polarization data with Tafel equation. Measurements were performed in deaerated 1.0 M KOH solution at 5.0 mV s^{-1} at room temperature: (1) -2.0 V, (2) -2.5 V, (3) -3.0 V, (4) -4.0 V *vs.* RHE.

It follows from **Figures 2(a)** that the cathodic current density associated with the HER enhances with increasing the polarization potential time, t_{pp}. The cathodic current also increases as the pre-polarization potential is made more negative (from -2.0 to -4.0 V *vs.* RHE), **Figure 3(a)**. This effect suggests that the electrocatalytic properties of the cathode (catalyst) surface induced by the evolution of hydrogen are modified: the initial surface has inferior catalytic performance, and the reduction process of water molecules is extremely slow. However, after cathodic activation, the reduction of water molecules, and hence the HER kinetics, at the cathode surface is prompted. The catalyst is, therefore, activated upon cathodic pre-treatment. In the near-surface area, it is plausibly related to hydrogen incorporation into the CF lattice. A similar effect has been previously reported in our laboratory for hydrogen evolution on various nanostructured materials [24-27].

The various electrochemical parameters, describing the kinetics of the HER, associated with such polarization measurements are depicted in the **Table 2**.

Table 2. Electrochemical HER kinetic parameters recorded for CF under various cathodic pre-treatment conditions. Measurements were performed at room temperature in deaerated KOH solution (1.0 M) at 5.0 mV s^{-1}. Double layer capacitance (C_{dl}) and electrochemical active surface area (EASA) values were determined from the non-Faradaic capacitive current associated with double-layer charging from the cyclic voltammetry measurements conducted at various scan rates (20-120 mV s^{-1}).

Cathodic pre-polarization conditions applied to the CF/OH^- interface	Cathodic pre-treatment parameters	$-E_{HER}$ / mV *vs.* RHE	$-b$ / mV dec^{-1}	j_o / mA cm^{-2}	η_{10} / mV	C_{dl} / mF cm^{-2}	EASA / cm^2
Effect of pre-polarization time (t_{pp}): holding the electrode at -2.0 V *vs* RHE for various t_{pp} values	t_{pp} = 0.0 h	810	290	5.6×10^{-3}	890	4.75	118.75
	t_{pp} = 0.5 h	800	253	4.9×10^{-3}	870	6.70	167.5
	t_{pp} = 2.0 h	610	332	6.3×10^{-2}	725	11.61	290.25
	t_{pp} = 4.0 h	530	320	8.9×10^{-2}	640	18.99	474.75
	t_{pp} = 12 h	386	175	2.95×10^{-2}	440	28.68	717.0
Effect of cathodic potential (E_c): the electrode is held for 12 h at various E_c values	E_c = -2.5 V *vs.* RHE	260	126	3.55×10^{-2}	295	37.66	941.5
	E_c = -3.0 V *vs.* RHE	205	110	5.0×10^{-2}	240	44.43	1110.8
	E_c = -4.0 V *vs.* RHE	157	90	9.7×10^{-2}	182	48.52	1213.0

These HER kinetic parameters are extracted through fitting the experimental polarization data, **Figures 2(a) and 3(a)**, to the Tafel equation yielding the Tafel plots depicted in **Figures 2(b)** and **3(b)**. It is obvious, from the results of the **Table 2**, that the various cathodic pre-polarization conditions applied to the CF/KOH interface have a significant catalytic impact on the HER kinetics on CF. The nonactivated CF sample (t_{pp} = 0.0 and E_c = -2.0 V *vs.* RHE) exhibited inferior catalytic activity with a highly negative onset potential (E_{HER}) value of -810 mV *vs.* RHE. The E_{HER} values markedly drifted towards the less negative (active) direction, **Table 2**, when the CF sample was exposed to various cathodic polarization pre-treatment conditions (cathodic activation).

The HER catalytic activity of the CF samples was, therefore, significantly improved upon cathodic activation. The cathodically-activated CF samples' HER catalytic performance has increased to different extents, depending on the cathodic pre-polarization conditions applied to the CF/KOH interface. For instance, the E_{HER} value decreased from -810 mV *vs.* RHE for the nonactivated CF sample to -800, -610, -530, and -386 mV *vs.* RHE for the CF samples cathodically-activated by holding the CF sample at -2.0 V *vs.* RHE for t_{pp} values of 0.5, 2.0, 4.0, and 12 h, respectively. The E_{HER} value was further reduced from -386 mV for the CF sample cathodically activated for t_{pp} = 12 h at -2.0 V *vs.* RHE to -260, -205, and -157 mV *vs.* RHE for the samples cathodically-activated upon holding the CF sample at -2.5, -3.0, and -4.0 V *vs.* RHE for the same pre-polarization duration period, respectively.

Another important electrochemical parameter commonly employed for the comparison and assessment of the activities and performance of catalysts towards the HER is the overpotential the catalyst must acquire to deliver 10 mA cm^{-2}, η_{10} [28]. Like E_{HER}, reduced η_{10} values refer to enhanced catalytic activity. The value of η_{10} was found to decrease following exactly the same sequence exhibited by E_{HER}. It follows from **Table 2** that, at a constant applied potential (-2.0 V *vs.* RHE), the value of η_{10} decreases, corresponding to efficient hydrogen generation at lower overpotentials (i.e., enhanced catalytic activity), as t_{pp} becomes longer. Also, at a given t_{pp} (12 h), the value of η_{10} diminished as E_c was made more negative. These findings demonstrated the benefits of the cathodic polarization pre-treatment processes on the CF catalytic efficiency for the HER.

On the one hand, there is no definite variation or trend in the Tafel slopes (b), and hence in the j_o values estimated from the Tafel extrapolation method, for the CF samples cathodically-activated at -2.0 V *vs.* RHE for various t_{pp} values. On the other hand, at a constant t_{pp} value of

12h, there was an apparent decrease in the *b* values from 175 to 90 mV dec^{-1}, corresponding to increased j_o values from 2.95×10^{-2} to 9.7×10^{-2} mA cm^{-2}, upon increasing the applied cathodic potential (E_c) from -2.0 to -4.0 V *vs.* RHE. As lower Tafel slopes usually refer to profusion in the availability of active sites on the catalyst surface, this apparent decrease in *b* denotes prompted HER kinetics [4]. The lowest *b* value (90 mV dec^{-1}) and the highest j_o value (9.7×10^{-2} mA cm^{-2}) were recorded for the CF samples cathodically-activated at -4.0 V *vs.* RHE for 12 h thus, highlighting its effective HER catalytic activity.

Comparing the *b* values estimated here (**Table 2**) with the theoretical ones listed below in the **Eqs. (1-3)**, which illustrates the path of the HER in alkaline electrolytes on a particular catalyst [29], will enable us to understand the HER key mechanism under these conditions.

$$H_2O + e^- \rightarrow H_{ads} + HO^- \qquad \text{(Volmer step)} \qquad (1)$$

$$b = \frac{2.34\mathrm{RT}}{\alpha \mathrm{F}} \cong 120\ \mathrm{mV/dec}$$

The Volmer step is followed by either the desorption Heyrovsky step:

$$H_2O + e^- + H_{ads} \rightarrow H_2 + HO^- \qquad \text{(Heyrovsky)} \qquad (2)$$

$$b = \frac{2.34\mathrm{RT}}{2\mathrm{F}} \cong 40\ \mathrm{mV/dec}$$

or a combination of adsorbed species to form molecular H_2:

$$H_{ads} + H_{ads} \rightarrow H_{2ads} \qquad \text{(Tafel step)} \qquad (3)$$

$$b = \frac{2.34\mathrm{RT}}{(1+\alpha)\mathrm{F}} \cong 30\ \mathrm{mV/dec}$$

The *b* values estimated for the two CF samples cathodically-activated for 12 h at -2.5 and -3.0 V *vs.* RHE (110 and 126 mV dec^{-1}), which are close to the standard *b* value of 120 mV dec^{-1}, suggest the Volmer step, Eq. (1), as the main step controlling the HER. The HER kinetics of the other activated CF samples are limited by the ineffectual number of catalytically active sites on which H_{ads} species form [4, 29], indicated by their high *b* values (175-332 mV dec^{-1}). On the other hand, the decreased *b* value (90

mV dec^{-1}) of the CF sample exposed to 12 h of cathodic activation at a high potential of -4.0 V *vs.* RHE catalyst infers that the number of active sites available on the catalyst surface has increased, resulting in enhanced HER kinetics [16, 24-27].

3. Long-term stability tests

Various electrochemical techniques performed under severe cathodic conditions were applied to the CF/KOH interface to evaluate the CF catalyst's sustainability. These techniques include continued potential cycling (up to 10,000 cycles) and chronoamperometry (current against time at a given potential).

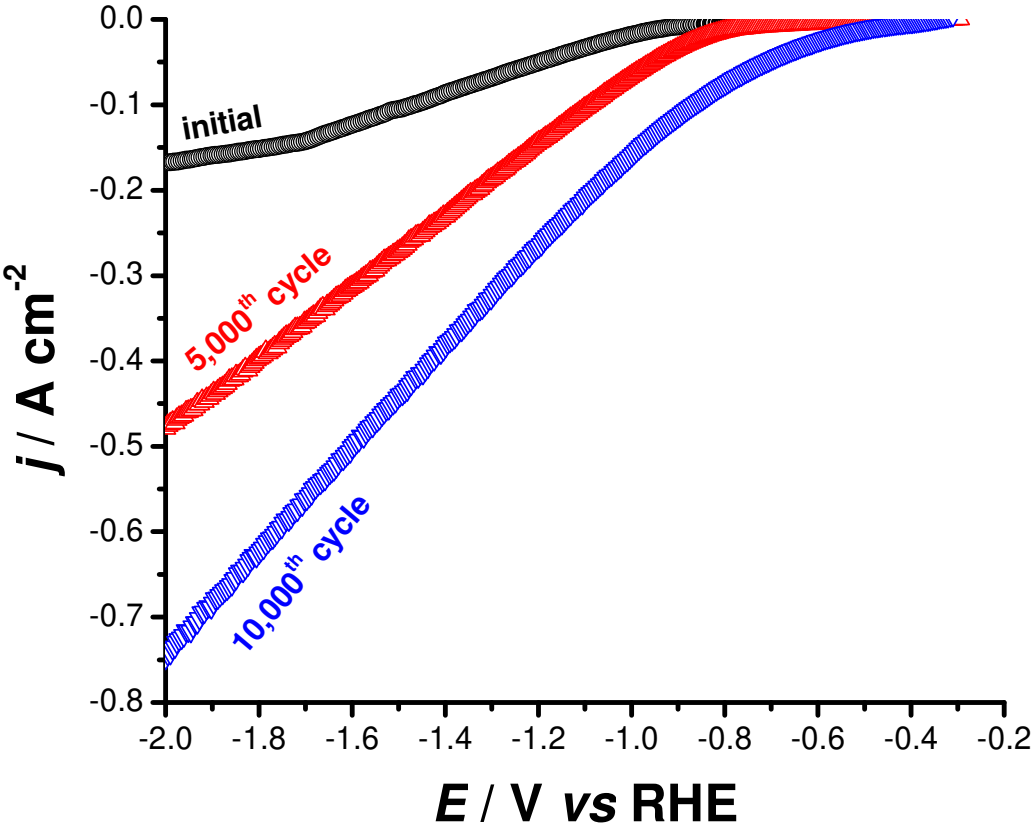

Figure 4. Long-term stability test of the CF sample (as-received) performed under repetitive cycling (10,000 cycles). Measurements were performed in deaerated 1.0 M KOH aqueous solution at 25 ºC.

The polarization curves of the catalyst indicate significant changes towards higher cathodic currents after 5,000 and 10,000 cycles, as seen in **Figure 4**. This rise in current after potential cycling affirms the activation of the CF catalyst observed during

polarization measurements conducted under various pre-polarization conditions (revisit **Figures 1-3**). This activation enhances as the cathodic potentials goes to the more negative values, as hydrogen evolves abundantly at the higher cathodic potentials.

The catalyst was also subjected to a prolonged chronoamperomery (current *vs.* time at a constant cathodic potential), **Figure 5**, and chronopotentiometry (potential *vs.* time at a given cathodic current), **Figure 6**, tests for 24 h to further assess its stability and durability.

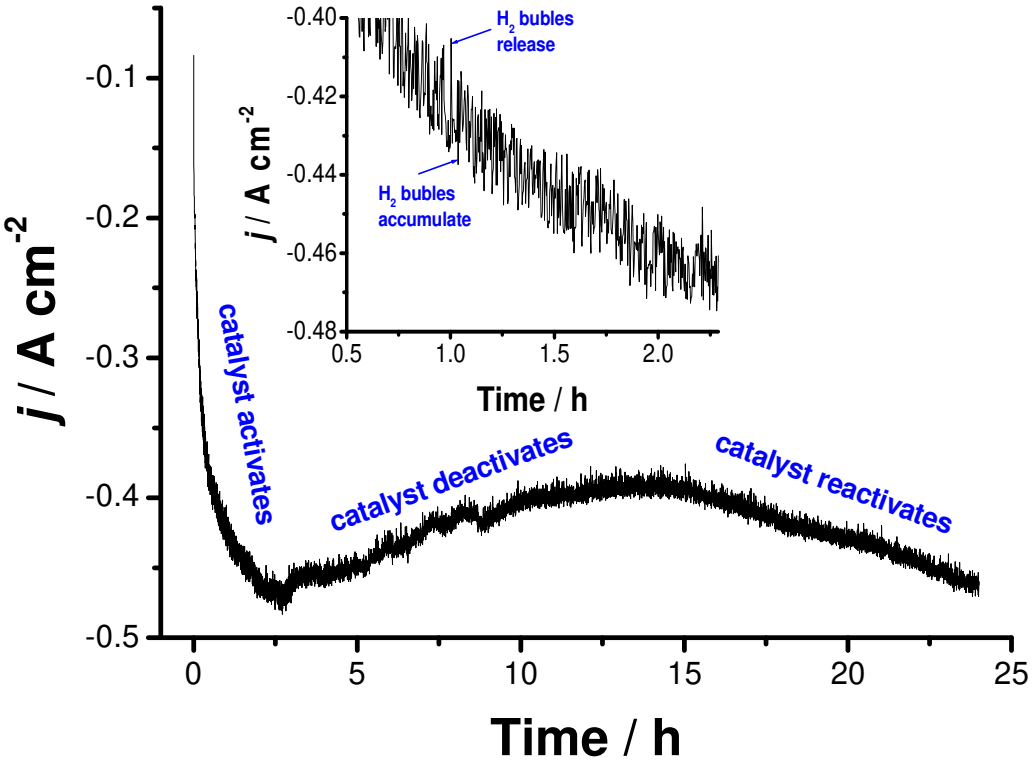

Figure 5. Chronoamperometry plot of bare carbon felt polarized at -2 V *vs.* RHE in 1.0 M KOH.

Within the first 10 min of the operation, the current suddenly falls down towards the more negative (active) values from an instantaneous (initial) current value of -0.08 A cm^{-2} to -0.3 A cm^{-2}, indicating fast activation of the catalyst. The current continues to shift to more negative values, but at a slower rate till reaching its maximum value (-0.47 A cm^{-2}), and oscillations in current start to appear. Then it decreased slowly,

attaining its minimum value (-0.4 A cm^{-2}) at t~14 h. This minimum current value (-0.4 A cm^{-2}) is still lower (more negative) than that of the instantaneous current (-0.08 A cm^{-2}), meaning that the catalyst is partly deactivated. The catalyst's partial deactivation at this stage is most probably due to blocking of some active sites by the accumulation of H_2 bubbles. The cathodic current then rises again (catalyst reactivation) with almost the same slope to -0.46 A cm^{-2}, forming a broad hump with a small height.

The current oscillations are characteristics of a continued competition between two processes, namely the release and accumulation of H_2 bubbles [26, 30]. The aggregation of bubbles during H_2 piling up is anticipated to separate the catalyst's active sites in the electrolyte from the electroactive species, hindering the transfer of charge and thus, decreases the current (catalyst deactivation). The current is then strengthened by the liberation of gas (catalyst reactivation), leaving the active sites free for a new H_2O molecule reduction process [26, 30]. The accumulation/release process of H_2 bubbles is replicated in a very short time (Inset in **Figure 5**), resulting in the manifestation of current noise. In spite of the continuous competition between the liberation of H_2 bubbles and accumulation processes, the net result is an increase in the cathodic current throughout the run, denoting catalyst activation during the operation.

During the long-term electrolysis test at high cathodic overpotential, where hydrogen is profusely released, hydrogen is postulated to integrate into the catalyst's crystal lattice, creating new catalytically active sites for water molecules' reduction [26, 30]. Hydrogen incorporation into the catalyst's structure is turned into a marked increase in the catalyst's electrochemical active surface area (EASA). This is manifested from the catalyst surface's electrochemical double-layer capacitance (C_{dl}), calculated from the non-Faradaic capacitive current, associated with double-layer charging from the cyclic voltammograms [31, 32]. CV measurements were performed

for each cathodically-activated CF sample, see **Figure 6** as a representative example. The rest of the CV data are shown in **Figures S1-S8 (Supporting Information)**, and the calculated values of C_{dl} and EASA are also reported in **Table 2**.

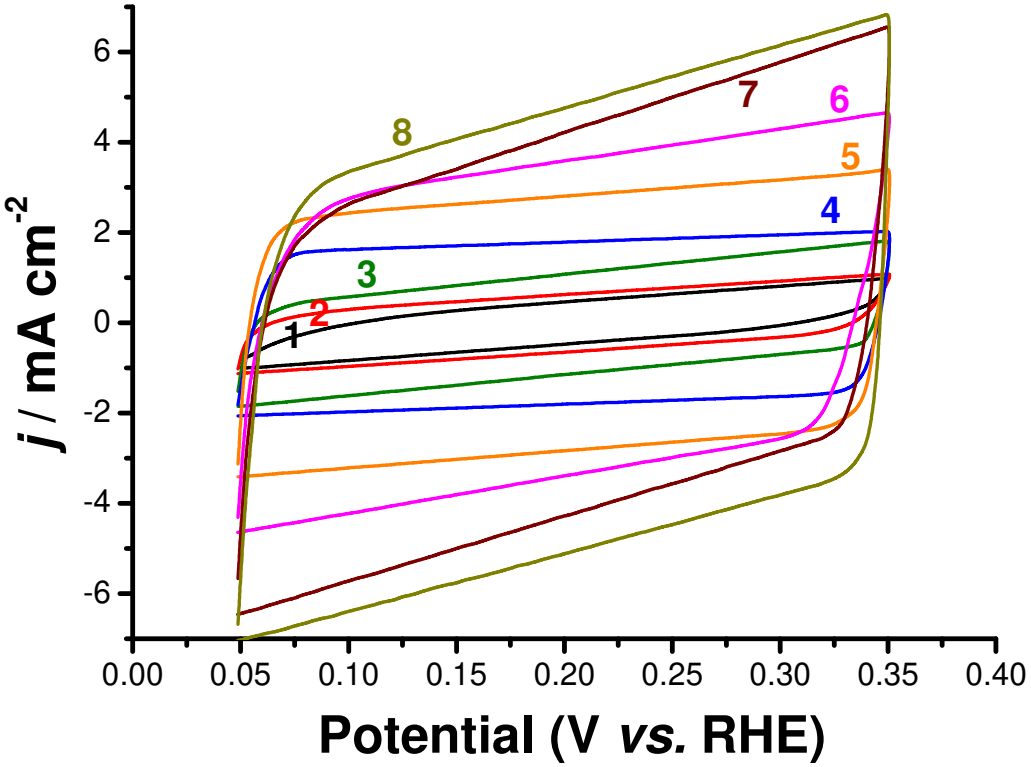

Figure 6. Cyclic voltammograms of as-received CF samples, before (curve 1) and after cathodic pre-polarization conditions (curves 2-8), recorded in a non-Faradaic region of the voltammogram for determining the catalyst's electrochemically-active surface area. Measurements were performed in deaerated KOH solution (1.0 M) at 100 mV s^{-1} at room temperature. (1) as-received (inactivated) CF; cathodically activated CF samples: (2) t_{pp} = 0.5h @ E_c = -2.0 V *vs.* RHE; (3) t_{pp} = 2.0h @ E_c = -2.0 V *vs.* RHE; (4) t_{pp} = 4.0h @ E_c = -2.0 V *vs.* RHE; (5) t_{pp} = 12h @ E_c = -2.0 V *vs* RHE; (6) t_{pp} = 12h @ E_c = -2.5 V *vs.* RHE; (7) t_{pp} = 12h @ E_c = -3.0 V *vs.* RHE; (8) t_{pp} = 12h @ E_c = -4.0 V *vs.* RHE.

The slopes of the anodic and cathodic charge currents measured at -0.20 V *vs.* RHE against the potential scan rate plots give the $(C_{dl})_{anodic}$ and $(C_{dl})_{cathodic}$ values, **Figures S1(b)-S8(b) (Supporting Information)**. The catalyst's C_{dl} value is taken as the average of the absolute value of both $(C_{dl})_{anodic}$ and $(C_{dl})_{cathodic}$, **Table 2**. It is obvious from the results in **Table 2** that the value of C_{dl} markedly increased upon cathodic activation to an extent relying on the cathodic pre-polarization treatment applied to the CF/KOH interface. For example, it

increased from 4.75 mF cm^{-2} for the nonactivated CF sample to 6.7, 11.61, 18.99, and 28.68 mF cm^{-2} for the CF samples after 0.5, 2, 4, and 12 h of cathodic activation at -2.0 and -4.0 V *vs.* RHE, respectively. At a given t_{pp} (12 h), the value of C_{dl} is further increased as the applied cathodic potential was more negative. It increased from 28.68 mF cm^{-2} at E_c = -2.0 V *vs.* RHE to 37.66, 44.43, and 48.52 mF cm^{-2} at E_c values of -2.5, -3.0, and -4.0 V *vs.* RHE, respectively. These findings confirmed the beneficial impact of the cathodic activation process, since electrocatalysts with higher C_{dl} values possess plenty of attainable active surface sites [33-35].

This, in turn, expedites efficacious charge transfer, leading to high catalytic performance. EIS measurements (**Supporting Information**, **Figures S9**, with a suitable equivalent circuit depicted in **Figure S10**) supported the enhanced charge transfer upon cathodic activation.

Equation (4) is used to calculate the value of EASA before and after cathodic activation, considering 40 μF cm^{-2} as the average specific capacitance (C_s) value for a typical flat electrode (1.0 cm^2) [36]:

$$EASA = C_{dl} / C_s \quad (4)$$

Based on Eq. (4), the highest EASA value (1213.00 cm^2) was determined for the CF sample after exposure to 12 h of cathodic pre-polarization at -4.0 V *vs.* RHE. This value is 10 times greater than that of the untreated CF sample (118.75 cm^2).

The obvious increase in the C_{dl} values upon cathodic activation indicates some contribution from the highly active surface area of the cathodically activated CF catalysts, as evidenced from the EASA values (**Table 2**). However, there is also a significant improvement in the cathodic current density among the studied cathodically activated CF samples (revisit **Figures 2** and **3**). This suggests that the cathodically activated CF samples' superior HER catalytic performance cannot be solely attributed to the change of active surface area, but also

to the structural changes that occurred at the atomic level, as a result of the process of cathodic activation.

To gain further insight into the high intrinsic catalytic activity of the cathodically activated CF samples, the number of active sites *n* were determined using Eq. (5) [37]:

$$n = Q/2F \quad (5)$$

where *Q* is the catalyst's voltammetry charge determined from the CV measurements, **Figure 6**. The number 2 refers to the number of electrons consumed during the HER reaction, and *F* is the Faraday's constant (96485 C/mol). **Table S1** (**Supporting Information**) depicts the values of *Q* and *n* recorded for the cathodically-activated CF samples in a comparison with the inactivated (as-received) one. Results revealed that, at a constant applied potential (E_c = -2.0 V *vs.* RHE), the value of *n* increases with increasing t_{pp}, and further increases at a given t_{pp} (12 h) as E_c was held at more cathodic values.

To determine the per-site turnover frequencies (TOFs, s^{-1}), the formula depicted in Eq. (6) is used.

$$\text{TOF} = |I| / 2Fn \quad (6)$$

where I is the current value (A cm^{-2}) measured at a specific overpotential. Merging Eqs. (2) and (3) yields Eq. (7):

$$\text{TOF} = | I | / Q \quad (7)$$

It is therefore possible, based on Eq. (7), to turn the current densities obtained from LSV measurements into TOF values, **Figures S11 and S12** (**Supporting Information**).

It is inferred from **Figures S11 and S12** that, for any investigated catalyst, the TOF value increases as the voltage applied to the CF/KOH interface is made more cathodic, where H_2 gas is excessively released. At any applied voltage, particularly at high negative values, the value of TOF is found to enhance with t_{pp}. At a given t_{pp} (12 h), significant increase in TOF is observed when the CF sample is subjected to cathodic activation under high negative E_c

values. These results add additional evidence for the remarkable catalytic role of the various cathodic pre-polarization processes applied to the CF/OH^- interface in catalyzing the alkaline HER.

In order to further compare the HER electrocatalytic performance, the investigated cathodically-activated CF catalysts' Faradaic efficiency (*FE%*) is calculated. Detailed calculations are shown in ***Section* S1.4** (**Supporting Information**), and **Table 3** collects the data obtained, namely the estimated and measured volumes of H_2 produced through the applied electrolysis process. Results show that the value of *FE%* increases with increasing t_{pp} at a constant cathodic potential (E_c = -2.0 V *vs.* RHE), and further increased at a given t_{pp} (12 h) as E_c was kept at more cathodic values. The CF sample cathodically-activated at E_c = -4.0 V for 12 h is also reported here as the most active catalyst for the HER among the other activated samples tested, as it recorded the largest amount of H_2 (32.66 μmol h^{-1}) measured by GC with an *FE%* value of 98.78%. These results highlight the outstanding HER catalytic activity of the CF catalyst cathodically-activated at -4.0 V *vs.* RHE for 12 h, which is analogous to the catalytic performance of the most efficacious metal-free electrocatalysts for HER published in the literature (**Supporting Information**, **Table S2**).

Table 3. Mean value (standard deviation) of V_{H2} (measured and calculated) after 1 h of a controlled galvanostatic electrolysis (CGE)*, along with the Faradaic Efficiency values, ε(%), for the investigated catalysts.

Cathodic pre-polarization conditions applied to the CF/OH^- interface	Cathodic pre-treatment parameters	H_2 measured by GC (H_2 / μmol h^{-1})	Calculated H_2 based on the charge passed during electrolysis		*FE*(%)
			Charge passed / C	H_2 / μmol h^{-1}	
Effect of pre-polarization time (t_{pp}): holding the electrode at -2.0 V *vs.* RHE for various t_{pp} values	t_{pp} = 0.0 h	12.72(0.15)	3.02(0.04)	15.65(0.2)	81.3(1.05)
	t_{pp} = 0.5 h	15.14(0.18)	3.4(0.048)	17.62(0.33)	85.9(1.12)
	t_{pp} = 2.0 h	18.02(0.25)	3.88(0.05)	20.11(0.38)	89.6(1.2)
	t_{pp} = 4.0 h	21.98(0.30)	4.6(0.07)	23.84(0.42)	92.2(1.3)
	t_{pp} = 12 h	26.80(0.40)	5.4(0.10)	27.98(0.55)	95.8(1.2)
Effect of cathodic potential (E_c): the electrode is held for 12 h at various E_c values	E_c = -2.5 V *vs.* RHE	28.84(0.45)	5.77(0.11)	29.90(0.6)	96.44(1.4)
	E_c = -3.0 V *vs.* RHE	30.03(0.50)	5.96(0.11)	30.89(0.62)	97.2(1.35)
	E_c = -4.0 V *vs.* RHE	32.66(0.53)	6.38(0.12)	33.06(0.65)	98.78(1.5)

* *CGE: the catalyst is held at a current density of -10 mA cm^{-2} for 1 h in 1.0 M KOH solution at 25 °C.*

Characterization of the CF samples before and after cathodic activation

To gain some insights on the impact of the cathodic activation, the morphology of the CF samples before and after polarization at -2 V for 12 h in 1.0 M KOH was assessed using scanning electron microscopy (SEM). **Figure 7a** displays the SEM image of non-treated CF sample consisting of carbon fibers (~2 μm in diameter) arranged in form of bundles with an average size of 10 μm. The magnification SEM image revealed smooth fiber walls with a few protrusions (**Fig. 7b**). After cathodic activation, there was no obvious change in the surface morphology, although a significant number of small humps is apparent at high magnification

(**Fig. 7d**). These humps could explain the increased electrochemical surface area recorded after cathodic polarization and thus improved electrocatalytic performance for HER. From these observations, one could infer that the electrochemical activation did not affect the bulk of the fibers and any change that occurred during this process was limited to the CF surface. The results are in accordance with the high corrosion stability of the CF in different media [22].

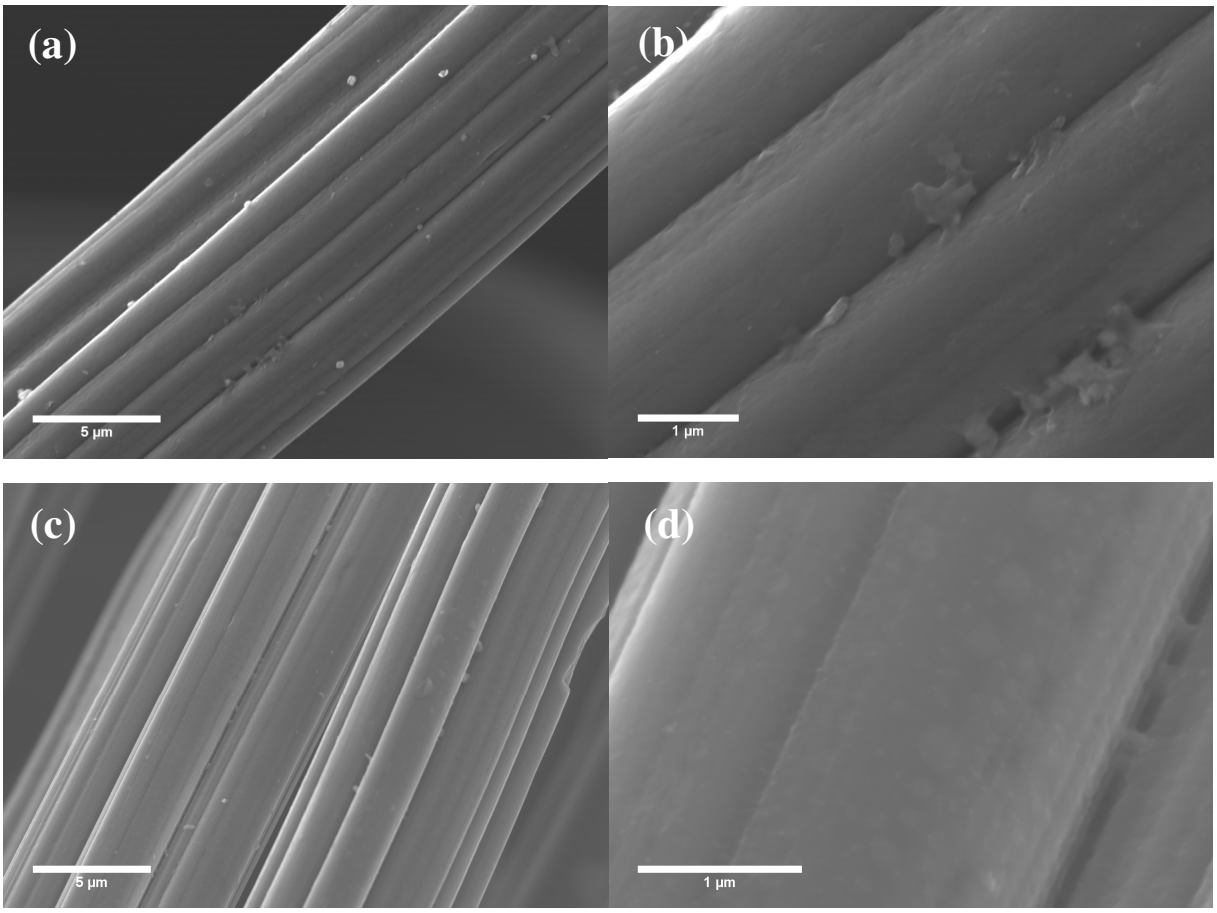

Figure 7. SEM images at different magnifications of carbon felt samples before (**a, b**), and after cathodic activation (**c, d**).

Energy dispersive X-ray (EDX) analysis of the CF samples was further conducted to examine the chemical changes that took place during the cathodic activation in 1.0 M KOH (**Table S3**). The results revealed a small increase of the oxygen content from 0.30 to 0.48 at.% after cathodic activation, which is in accordance with a surface-confined process. Indeed,

EDX provides chemical information of the bulk material, while the electrochemical activation process is believed to occur essentially on the CF surface.

EDX mapping showed homogeneous distribution of carbon and oxygen throughout the CF surface before and after cathodic polarization at -2 V for 12 h in 1.0 M KOH (**Figure S13**).

The chemical composition of the CF samples was further probed through X-ray photoelectron spectroscopy (XPS) analysis to gain more insight on chemical changes that have occurred on the CF surface upon electrochemical activation. **Figure S14** depicts the XPS survey spectra of the CF samples before and after cathodic activation. Both spectra contain only carbon and oxygen, in full agreement with their chemical composition. It is worth to notice that the amount of oxygen increased from 6.17 to 9.66 at.% after cathodic activation, implying, as expected, an oxidation of the surface (**Table S4**). The result is in full accordance with EDS analysis.

The core level XPS spectrum of the C_{1s} region of the initial (non-activated) CF sample is exhibited in **Figure 8a**. It can be curve-fitted with four different peaks at 282.8 eV (metal carbide), 284.0 eV (Csp^2), 285.0 eV (Csp^3) and 287.9 eV (C=O) with the main peak being that ascribed to graphitic carbon at 284.0 eV. After cathodic activation, the C_{1s} core level spectrum obviously experienced a significant change. It can be fitted with four bands at 283.6, 285.0, 286.4 and 288.2 eV assigned respectively to Csp^2, Csp^3/C-H, C-O and C=O groups. The significant increase of the Csp^3 upon cathodic polarization in 1.0 M KOH aqueous solution could be due to partial hydrogenation of the C=C top surface bonds even though this chemical transformation generally occurs at high temperature under metal catalysis.

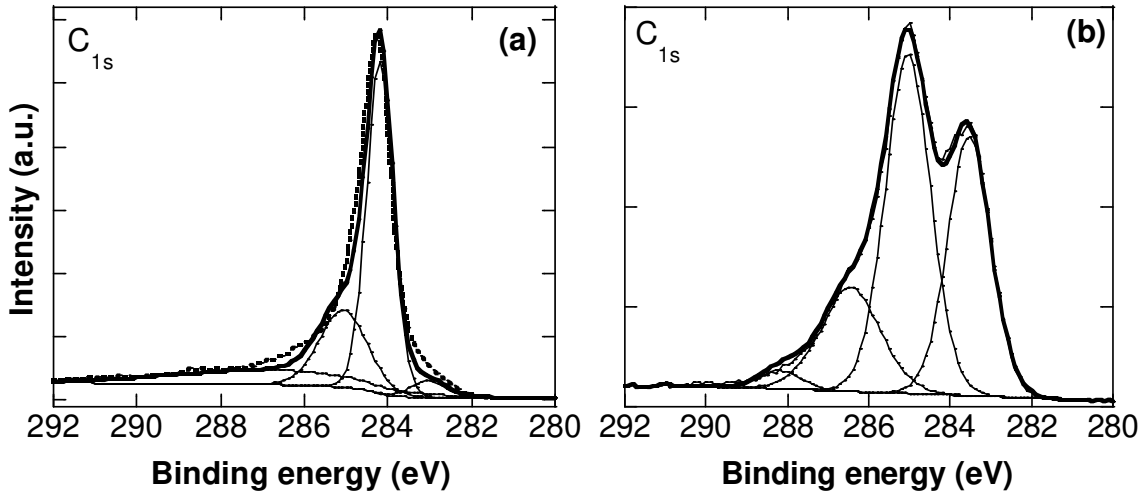

Figure 8. Core level XPS spectra of the C_{1s} of CF before (**a**) and after (**b**) cathodic activation (t_{pp} = 24h @ -2.0 V *vs* RHE).

Raman spectroscopy is valuable tool for the characterization of carbon-based materials. **Figure 9** displays the Raman spectra of the CF before and after cathodic activation in KOH (1.0 M) for 12 h. Both spectra comprise two main bands at around 1354 and 1580 cm^{-1} characteristic respectively of D- and G-bands. While the D-band is assigned to structural defects/disorder within the carbon network, the G-band is ascribed to graphitic carbon. The I_D/I_G ratio is usually used to assess the evolution of the defects in carbon-based materials. While the I_D/I_G ratio of the initial CF was ~0.98, the value decreased slightly to 0.92 after cathodic activation. This decrease of I_D/I_G ratio is in favor of diminution of defects and disorder in the CF structure after cathodic activation [38]. The other bands at about 2692, 2933 and 3225 cm^{-1} are commonly assigned to 2D, D+G and 2D', respectively [39]. Again, the Raman analysis agrees well with a process affecting the surface properties rather than bulk.

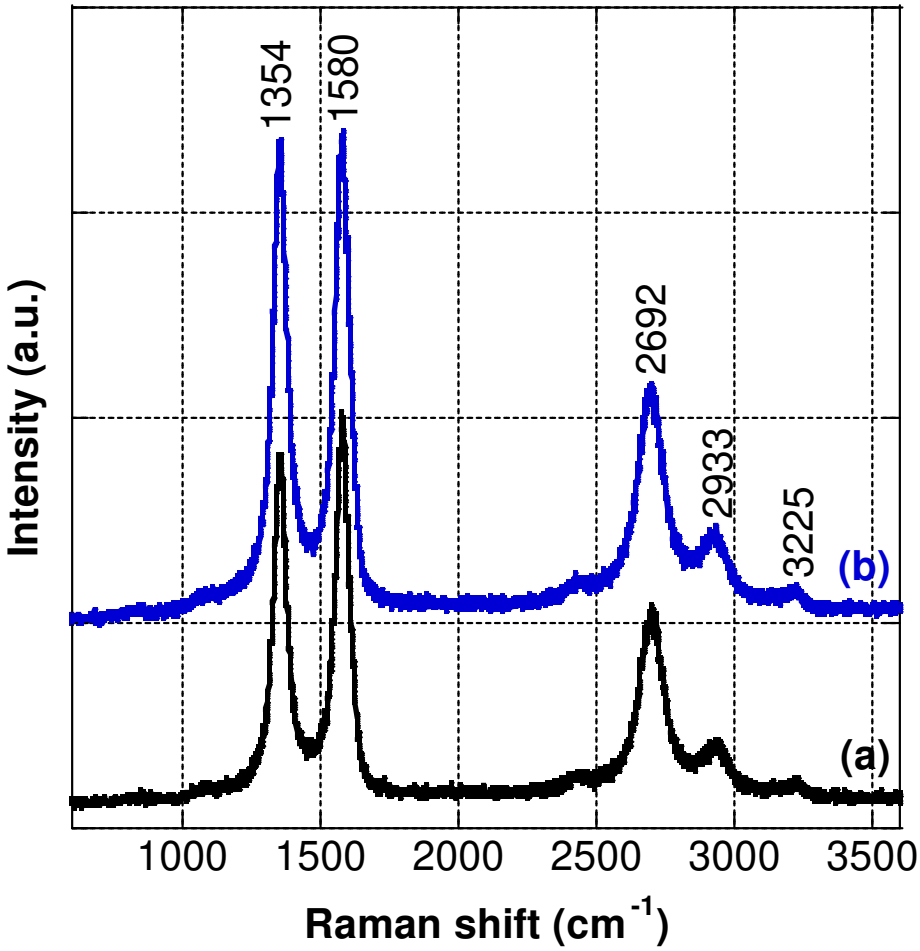

Figure 9. Raman spectra of the CF before (a) and after (b) cathodic activation (t_{pp} = 24h @ -2.0 V *vs.* RHE).

4. Conclusion

The results gathered in the present study demonstrated that the electrocatalytic properties of carbon felt (CF) can be improved through a simple cathodic activation process in KOH (1.0 M) aqueous solution. Under optimized operating conditions, i.e. applied voltage and polarization time, the catalytic performance for the hydrogen evolution reaction (HER) was drastically enhanced. Under metal-free conditions, the cathodically activated CF recorded a current density of 10 mA cm^{-2} at an overpotential of 180 mV *vs.* RHE and a long-term stability. This performance was achieved under experimental conditions that did not require huge investment as the activation process was conducted in the same electrochemical cell and

electrolyte solution used for HER measurements. Under our experimental conditions, X-ray photoelectron spectroscopy analysis revealed surface oxidation. The formation of oxygen-containing groups on the CF surface are believed to enhance water adsorption and act as active sites for hydrogen generation. Taken together the findings in this study hold promise for the development of metal-free electrodes that can operate in alkaline media with a performance that could challenge the most commonly used noble-metal free catalysts.

Acknowledgements

The authors gratefully acknowledge financial support from the Centre National de la Recherche Scientifique (CNRS), the University of Lille, and the Hauts-de-France region. The authors are also thankful to the Taif University Researchers Supporting Project number (TURSP-2020/03), Taif University, Taif, Saudi Arabia.

Conflict of interest

No conflict of interest to declare.

4. References

[1] I. Dincer, C. Acar, A review on clean energy solutions for better sustainability, Int. J. Energy Res., 39 (2015) 585-606.

[2] L. Peng, Z. Wei, Catalyst engineering for electrochemical energy conversion from water to water: Water electrolysis and the hydrogen fuel cell, Engineering, 6 (2020) 653-679.

[3] A. Lasia, Handbook of Fuel Cells, Eds.; John Wiley & Sons, Ltd ed., Chechester, 2010.

[4] T. Shinagawa, A. T. Garcia-Esparza, K. Takanabe, Insight on Tafel slopes from a microkinetic analysis of aqueous electrocatalysis for energy conversion, Sci. Rep., 5 (2015) 13801.

[5] C. Hu, Y. Xiao, Y. Zou, L. Dai, Carbon-based metal-free electrocatalysis for energy conversion, energy storage, and environmental protection, Electrochem. Energy Rev., 1 (2018) 84-112.

[6] J. Wang, H. Kong, J. Zhang, Y. Hao, Z. Shao, F. Ciucci, Carbon-based electrocatalysts for sustainable energy applications, Progress Mater. Sci., (2020) https://doi.org/10.1016/j.pmatsci.2020.100717.

[7] X. Liu, L. Dai, Carbon-based metal-free catalysts, Nature Rev. Mater., 1 (2016) 1-12.

[8] L. Zhang, Y. Jia, X. Yan, X. Yao, Activity origins in nanocarbons for the electrocatalytic hydrogen evolution reaction, Small, 14 (2018) 1800235.

[9] X. Shang, J.-H. Tang, B. Dong, Y. Sun, Recent advances of nonprecious and bifunctional electrocatalysts for overall water splitting, Sustain. Energy Fuels, 4 (2020) 3211-3228.

[10] Y. Zhou, G. Chen, J. Zhang, A review of advanced metal-free carbon catalysts for oxygen reduction reactions towards the selective generation of hydrogen peroxide, J. Mater. Chem. A, 8 (2020) 20849-20869.

[11] M. D. Bhatt, J. Y. Lee, Advancement of platinum (Pt)-free (non-Pt precious metals) and/or metal-free (non-precious-metals) electrocatalysts in energy applications: A review and perspectives, Energy Fuels, 34 (2020) 6634–6695.

[12] P. P. Prosini, A. Pozio, S. Botti, R. Ciardi, Electrochemical studies of hydrogen evolution, storage and oxidation on carbon nanotube electrodes, J. Power Sources, 118 (2003) 265-269.

[13] R. K. Das, Y. Wang, S. V. Vasilyeva, E. Donoghue, I. Pucher, G. Kamenov, H.-P. Cheng, A. G. Rinzler, Extraordinary hydrogen evolution and oxidation reaction activity from carbon nanotubes and gaphitic carbons, ACS Nano, 8 (2014) 8447-8456.

[14] W. Cui, Q. Liu, N. Cheng, A. M. Asiri, X. Sun, Activated carbon nanotubes: a highly-active metal-free electrocatalyst for hydrogen evolution reaction, Chem. Commun., 50 (2014) 9340-9342.

[15] L. Wei, H. E. Karahan, K. Goh, W. Jiang, D. Yu, O. Birer, R. Jiang, Y. Chen, A high-performance metal-free hydrogen evolution reaction electrocatalyst from bacterium derived carbon, J. Mater. Chem. A, 3 (2015) 7210-7214.

[16] G. Darabdhara, M. A. Amin, G. A. M. Mersal, E. M. Ahmed, M. R. Das, M. B. Zakaria, V. Malgras, S. M. Alshehri, Y. Yamauchi, S. Szunerits, R. Boukherroub, Reduced graphene oxide nanosheets decorated with Au, Pd and Au–Pd bimetallic nanoparticles as highly efficient catalysts for electrochemical hydrogen generation, J. Mater. Chem. A, 3 (2015) 20254-20266.

[17] D. D. Demir, A. Salcı, R. Solmaz, Fabrication of Mo-modified carbon felt as candidate substrate for electrolysis: Optimization of pH, current and metal amount, Int. J. Hydrogen Energy, 43 (2018) 10540-10548.

[18] D. D. Demir, A. Salcı, R. Solmaz, Preparation, characterization and hydrogen production performance of MoPd deposited carbon felt/Mo electrodes, Int. J. Hydrogen Energy, 43 (2018) 10530-10539.

[19] M. B. Koca, G. G. Celik, G. Kardas,, B. l. Yazıcı, NiGa modified carbon-felt cathode for hydrogen production, Int. J. Hydrogen Energy, 44 (2019) 14157-14163.

[20] D. S. Dmitriev, N. A. Khristyuk, V. I. Popkov, Electrodeposition of α-Ni/β-Co composite coatings on the carbon felt: Structural features and electrochemical performance, J. Alloys Compds., 849 (2020) 156625.

[21] H. Yoon, H. J. Song, B. Ju, D.-W. Kim, Cobalt phosphide nanoarrays with crystalline–amorphous hybrid phase for hydrogen production in universal-pH, Nano Res., 13 (2020) 2469–2477.

[22] M. Mitov, E. Chorbadzhiyska, R. Rashkov, Y. Hubenova, Novel nanostructured electrocatalysts for hydrogen evolution reaction in neutral and weak acidic solutions, Int. J. Hydrogen Energy, 37 (2012) 16522-16526.

[23] A. Döner, I. Karcı, G. Kardas,, Effect of C-felt supported Ni, Co and NiCo catalysts to produce hydrogen, Int. J. Hydrogen Energy, 37 (2012) 9470-9476.

[24] N. Y. Mostafa, M. M. Qhtani, S. H. Alotaibi, Z. I. Zaki, S. Alharthi, M. Cieslik, K. Gornicka, J. Ryl, R. Boukherroub, M. A. Amin, Cathodic activation of synthesized highly defective monoclinic hydroxyl-functionalized ZrO_2 nanoparticles for efficient electrochemical production of hydrogen in alkaline media, Int. J. Energy Res., 44 (2020) 10695-10709.

[25] A. Mezni, M. M. Ibrahim, M. El-Kemary, A. A. Shaltout, N. Y. Mostafa, J. Ryl, T. Kumeria, T. Altalhi, M. A. Amin, Cathodically activated Au/TiO_2 nanocomposite synthesized by a new facile solvothermal method: An efficient electrocatalystwith Pt-likeactivity for hydrogen generation, Electrochim. Acta, 290 (2018) 404-418.

[26] G. Darabdhara, M. R. Das, M. A. Amin, G. A. M. Mersal, N. Y. Mostafa, S. S. Abd El-Rehim, S. Szunerits, R. Boukherroub, Au-Ni alloy nanoparticles supported on reduced grapheneoxide as highly efficient electrocatalysts for hydrogen evolution and oxygen reduction reactions, Int. J. Hydrogen Energy, 43 (2018) 1424-1438.

[27] M. A. Amin, S. A. Fadlallah, G. S. Alosaimi, F. Kandemirli, M. Saracoglu, S. Szunerits, R. Boukherroub, Cathodic activation of titanium-supported gold nanoparticles: An efficient and stable electrocatalyst for the hydrogen evolution reaction, Int. J. Hydrogen Energy, 41 (2016) 6326-6341.

[28] C. C. L. McCrory, S. Jung, J. C. Peters, T. F. Jaramillo, Benchmarking heterogeneous electrocatalystsfor the oxygen evolution reaction, J. Am. Chem. Soc., 135 (2013) 16977-16987.

[29] N. Mahmood, Y. Yao, J.-W. Zhang, L. Pan, X. Zhang, J.-J. Zou, Electrocatalysts for hydrogen evolution in alkaline electrolytes: Mechanisms, challenges, and prospective solutions, Adv. Sci., 5 (2018) 1700464.

[30] J. Xie, H. Zhang, S. Li, R. Wang, X. Sun, M. Zhou, J. Zhou, X. Wen Lou, Y. Xie, Defect-rich MoS_2 ultrathin nanosheets with additional active edge sites for enhanced electrocatalytic hydrogen evolution, Adv. Mater., 25 (2013) 5807-5813.

[31] J. D. Benck, Z. Chen, L. Y. Kuritzky, A. J. Forman, T. F. Jaramillo, Amorphous molybdenum sulfide catalysts for electrochemical hydrogen production: insights into the origin of their catalytic activity, ACS Catal., 2 (2012) 1916-1923.

[32] S. Trasatti, O. A. Petrii, Real surface area measurements in electrochemistry, Pure Appl. Chem., 63 (1991) 711-734.

[33] H. Zhou, F. Yu, Y. Huang, J. Sun, Z. Zhu, R. J. Nielsen, R. He, J. Bao, W. A. Goddard III, S. Chen, Z. Ren, Efficient hydrogen evolution by ternary molybdenum sulfoselenide particles on self-standing porous nickel diselenide foam, Nat. Commun., 7 (2016) 12765.

[34] M. Cabán-Acevedo, M. L. Stone, J. R. Schmidt, J. G. Thomas, Q. Ding, H.-C. Chang, M.-L. Tsai, Jr-H. He, S. Jin, Efficient hydrogen evolution catalysis using ternary pyrite-type cobalt phosphosulphide, Nat. Mater., 14 (2015) 1245-1251.

[35] H. Zhou, F. Yu, J. Sun, H. Zhu, I. K. Mishra, S. Chen, Z. Ren, Highly efficient hydrogen evolution from edge-oriented $WS_{2(1-x)}Se_{2x}$ particles on three-dimensional porous $NiSe_2$ foam, Nano Lett., 16 (2016) 7604-7609.

[36] JKibsgaard, T. F. Jaramillo, Molybdenum phosphosulfide: An active, acid-stable, earth-abundant catalyst for the hydrogen evolution reaction, Angew. Chem. Int. Ed., 53 (2014) 14433-14437.

[37] Y.-R. Liu, X. Shang, W.-K. Gao, B. Dong, J.-Q. Chi, X. Li, K.-L. Yan, Y.-M. Chai, Y.-Q. Liu, C.-G. Liu, Ternary CoS_2/MoS_2/RGO electrocatalyst with CoMoS phase for efficient hydrogen evolution, Appl. Surf. Sci., 412 (2017) 138-145.

[38] Y. Cheng, G. He, A. Barras, Y. Coffinier, S. Lu, W. Xu, S. Szunerits, R. Boukherroub, One-step immersion for fabrication of superhydrophobic/superoleophilic carbon felts with fire resistance: Fast separation and removal of oil from water, Chem. Eng. J., 331 (2018) 372-382.

[39] L. Bokobza, J.-L. Bruneel, M. Couzi, Raman spectra of carbon-based materials (from graphite to carbon black) and of some silicone composites, C J. Carbon Res., 1 (2015) 77-94.